Simulation of Internal Transport Barriers by the Canonical Profiles Transport Model (CPTM)

Yu.N. Dnestrovskij 1), S.V. Cherkasov 1), A.Yu. Dnestrovskij 1), S.E. Lysenko 1) and M.Walsh 2)

1) RRC "Kurchatov Institute", Nuclear Fusion Institute, Moscow, Russia
2) Walsh Scientific Ltd., Culham Science Centre, Abingdon, Oxfordshire, OX14 3EB, UK

e-mail contact of main author: dnyn@nfi.kiae.ru

Abstract. To describe the energy balance in the L-mode, the model containing the critical gradient is widely used. This so-called "first" critical gradient can be found in particular by the canonical profile for the temperature. For regimes with transport barriers we use the idea of the "second" critical gradient. If the pressure gradient exceeds the second critical gradient inside some plasma region, then the bifurcation to the new state is happened in this region with the formation of the transport barrier. This idea is realized in the modified canonical profiles model, suitable for the energy and particle balance simulation in tokamaks with arbitrary aspect ratio and plasma cross section. To choose the value of the second critical gradient, we compare the calculation results for several shots with experimental data. The connection of this gradient with the magnetic shear, s, is found. We obtained the following criterion of the transport barrier formation:$(a^2 /r)\, \mathrm{d}/\mathrm{d}r \ln(p/p_c) > z_0(r)$, where r is a radial coordinate, a is a minor radius of plasma, p and p_c are the plasma pressure and the canonical profile of the pressure, $z_0(r) = C_0 + C_1 s$ is the dimensionless function, which determines the "distance" between the first and the second critical gradients. $C_{0i} \sim 1$, $C_{0e} \sim 3$, $C_{1i,e} \sim 2$. Calculations have shown that this criterion is close to the experimental one obtained in JET. The constructed model was used for the simulation of the internal transport barriers in JET, TFTR, DIII-D and MAST. The possible dependence of the second critical gradient on plasma parameters is discussed also.

1. Introduction

To describe the energy balance in the L-mode, the models containing the critical gradients are widely used. These so-called "first" critical gradients can be found in particular by the canonical profile theory [1]. If the temperature and density gradients exceed the first critical gradients then the transport rises sharply due to the excitation of drift modes and increase of turbulent transport coefficients. In this state, the profiles of the temperature and pressure are close to the canonical ones and well conserved under any external actions (the profile consistency principle).

In this Report, to describe the regimes with Internal Transport Barriers (ITB) we use the idea of the "second" critical gradient. If the pressure gradient exceeds the second critical gradient inside some plasma region then the drift turbulence in this region is suppressed and the bifurcation to the new state occurs with the transport barrier formation. The plasma as if "forgets" the canonical profile inside the transport barrier.

The idea of the second critical gradient is realized in the canonical profiles transport model (**CPTM**), suitable for the energy and particle balance simulation in tokamaks with arbitrary aspect ratio and plasma cross-section. The model consists of a set of equations relative to the electron and ion temperatures, T_e, T_i, plasma density n and the potential of the poloidal magnetic field ψ. The equilibrium and the radial coordinate ρ are found by the solution of the Grad-Shafranov equation.

The first critical gradient is defined by the canonical profiles theory. The canonical profile for the function $\mu = 1/q$ (denoted below as μ_c) can be found by the solution of the Euler equation for the free plasma energy functional [1]

$$\rho^2 G\, \partial\mu_c^2/\partial\rho + (\lambda/2)\, \partial/\partial\rho\, ((1/V')\, \partial/\partial\rho(V'G\rho\mu_c)) = C\, \rho\mu_c'/V' \qquad (1)$$

The solution of Eq. (1) and the constants C and λ are determined by the following boundary conditions:

$$\mu_c(0) = \mu_0 \sim 1, \quad \mu_c'(0) = 0, \quad \mu_c(\rho_{max}) = \mu_S, \quad X \equiv [i_c/(2G\,\mu_c)]_S = \mu_S/\mu_0 \qquad (2)$$

Here index S means the plasma boundary, $i_c = 1/V'\, \partial/\partial\rho(G\, V'\rho\mu_c)$ is the dimensionless current density, V is the plasma volume, $V' = \partial V/\partial\rho$, $G = R^2\langle(\text{grad } \rho)^2/r^2\rangle$ is the metric coefficient. The first dimensionless critical gradients for the temperature and density are as follows:

$$\Omega_{Tc} = R/L_{Tc} \equiv -RT_c'/T_c = -\,2/3\, R\, i_c'/i_c,\ \Omega_{nc} \equiv -Rn_c'/n = -\,1/3\, R\, i_c'/i_c. \qquad (3)$$

Now let us consider the expressions for the heat and particle fluxes, Γ_α ($\alpha = e,i$), Γ_n:

$$\Gamma_\alpha = \kappa_\alpha T_\alpha/R\, (\Omega_{T\alpha}-\Omega_{Tc})\, H(\Omega_{T\alpha}-\Omega_{Tc})\, F_\alpha - \kappa_{0\alpha}\, \partial T_\alpha/\partial\rho + 3/2\, \Gamma_n T_\alpha\ (\alpha = e,i) \qquad (4)$$

$$\Gamma_n = D_n n/R\, (\Omega_n-\Omega_{nc})\, F_e F_i - D_0\kappa_{0\alpha}\, \partial n/\partial\rho, \qquad (5)$$

where $\Omega_{T\alpha} = -RT_\alpha'/T_\alpha$, $\Omega_n = -R\, n'/n$, κ_α, $\kappa_{0\alpha}$, D_n, D_0 are the heat diffusivity and particle diffusion coefficients [2]. The Heaviside function $H(x)$ in (4) describes an absence of heat pinch: $H(x) = 1$ ($x>0$), $H(x) = 0$ ($x<0$). The functions F_e, F_i (the forgetting factors) describe the bifurcation with the transport barriers formation. To determine these functions, we introduce the deviation of the partial pressure profile from the canonical one:

$$z_{p\alpha} = z_{p\alpha}(\rho) = (\rho_{max}/\rho)\, (\Omega_{p\alpha} - \Omega_{pc})\,/A, \qquad (\alpha = e,i) \qquad (6)$$

where $\Omega_{p\alpha} = -(R/p_\alpha)\, \partial p_\alpha/\partial\rho$, $\Omega_{pc} = -R\, i_c'/i_c$, $A = R/a$ is the aspect ratio. In our model the transport barrier is formed inside some region, if the value of $z_{p\alpha}(\rho)$ exceeds the distance between the first and second critical gradients, $z_{0\alpha}(\rho)$, in this region:

$$z_{p\alpha}(\rho) > z_{0\alpha}(\rho) \qquad (7)$$

To describe the bifurcation, the functions F_e и F_i can be chosen as follows:

$$F_\alpha = \exp[-z_{p\alpha}^2/(2(z_{0\alpha})^2)] \qquad (8)$$

It is seen that $F_\alpha \ll 1$ inside the barrier and $F_\alpha \sim 1$ outside it. To choose the value of $z_{0\alpha}$, we compare the calculation results with experimental data. This choice of $z_{0\alpha}$ is discussed below. It will be shown also that the criterion (7) for devices with moderate and tight aspect ratio is close to the experimental one

$$\rho_s/L_T > \rho^*_{ITB}, \qquad \rho^*_{ITB}(\text{JET}) = 0.014 \qquad (9)$$

obtained in JET [3]. The links of heat fluxes with temperature gradients and the values of $z_{p\alpha}$ and $z_{0\alpha}$ are shown in Fig. 1. To describe experiments with ITB in the devices with low and conventional aspect ratio, we modify the transport model proposed in [4].

2. Modification of the CPTM

2.1. Modified boundary condition for the canonical profile

The boundary conditions (2) are used to distinguish the Kadomtsev's-type solution and the other solutions of Eq. (1). In such a way we call the solution of Eq. (1), for which the ratio i_c'/i_c has a regular behaviour at the plasma edge. Note, that this ratio is defined through the first and second derivatives of the function $\mu_c(\rho)$. Since the critical gradient is proportional to i_c'/i_c, for the Kadomtsev's-type solution, the critical gradient is also regular at the edge.

The problem of the Kadomtsev's-type solution for tokamaks with low aspect ratio A=R/a is rather difficult, because the metric coefficient G (included in Eq. (1)) has very irregular behaviour at the plasma periphery. Figure 2 shows the profiles of G in tokamaks with various aspect ratios and moderate values of the edge safety factor q. For all cases $G(0)$ ~1, but for A=1.5 the value of G rapidly increases at the edge and attains the level of 10-15 for the plasma with rather high elongation. In this case the using of the boundary condition (2) for X results in a very irregular behaviour of i_c'/i_c. To distinguish the Kadomtsev's-type solution, we introduce the modified boundary condition instead of the last equality in (2)

$$X \equiv [i_c/(2G\,\mu_c)]_S = f(G_a)\,\mu_S/\mu_0\,, \quad f(G_a) = (G_a)^{\alpha}, \;\; \alpha = 0.4 - 0.6. \tag{10}$$

The calculations show that the $\mu_c(\rho)$ profile itself is only slightly changed, but the value of i_c'/i_c becomes regular at the edge. Figure 3 presents the profiles of the critical gradient Ω_{Tc}= $-RT_i'/T_i$ = -2/3 R i_c'/i_c for the cases $f(G_a)$ = 1 and $f(G_a) = (G_a)^{1/2}$. We see that the boundary condition (10) regularizes well the behaviour of the critical gradient. The comparison of the first critical gradients in three devices with different aspect ratios (T-10, JET and MAST) is carried out in Fig. 4. For T-10 and JET the factor $f(G_a)$ is slightly differs from unity, and the boundary conditions (2) and (10) are close to each other.

2.2. Modified transport model

In our papers [5, 6] to simulate ITB in JT-60U, we used the piecewise-linear functions for $z_{0\alpha}(\rho)$:

$$\begin{aligned} z_{0\alpha} &= C_{0\alpha} && 0<\rho<\rho_0 \\ z_{0\alpha} &= C_{0\alpha} + C_{1\alpha}\,(\rho - \rho_0)/\,(1 - \rho_0) && \rho_0<\rho<1, \end{aligned} \tag{11}$$

which contains two pairs of constants $C_{0\alpha}$ and $C_{1\alpha}$ for electrons (α = e) and for ions (α = i) correspondingly and the constant ρ_0. These constants were defined by comparison with experiment in JET, DIIID and JT-60U. The values of $z_{0\alpha}$ really define the magnitude of the second critical gradient to be overcome for the ITB formation. Note that the functions (11) are not linked with some physical parameters of the plasma.

It is well known that the negative shear helps to the formation of ITB. Therefore in our new model we suppose

$$z_{0\alpha} = C_{0\alpha} + C_{1\alpha} s\,, \tag{12}$$

where $s = \rho/q\;\partial q/\partial\rho$ is the magnetic shear. If the shear is positive, the spatial behaviour of functions (11) and (12) is similar: they monotonically grow. However, if the shear is negative, the function (12) may have a minimum, in the vicinity of which the bifurcation of solutions of transport equations is alleviated. Physically, this alleviates the ITB formation. Behaviour of functions $z_{0\alpha}(\rho)$ with negative shear is shown in Fig. 5.

In our calculations we use the expression (12). Really we solve the inverse problem relative to the parameters $C_{0\alpha}$ and $C_{1\alpha}$, comparing the calculation results with experimental data in the chosen shot. To validate the model, we compare the results obtained for different devices with the criterion (9) and make conclusions about the applicability of this criterion. The experimental data for JET, TFTR and DIII-D are taken from the ITER Database [7]. For MAST we used the ITER Database, MAST Database and Report [8].

3. Simulation of the JET shot #40847

Figure 6 shows the time behaviour of calculated and experimental values of the central ion and electron temperatures. The profiles of ion and electron temperatures at t = 46 sec are drawn in Fig. 7. Figure 8 shows the corresponding profiles of the heat diffusivities and density diffusion coefficient. It is well seen that all transport coefficient are very small in the gradient region. The comparison of the values of ρ_s/L_{Ti} for model calculations and experiment is carried out in Fig. 9. The sharp folds at the edges of the i-ITB are seen. At these points both in calculation and experiment $\rho_s/L_{Ti} \sim 0.01$, that is slightly less than criterion (9).

4. Simulation of the TFTR shot #94607

Figures 10-11 show the calculated and experimental profiles of temperatures T_i, T_e and density n. The calculated profiles of ρ_s/L_{Ti} for t = 2.11 sec and 2.23 sec and experimental one for t =2.23 sec are shown in Fig. 12. It is seen that ρ^*_{ITB}(TFTR) ~ 0.008 that almost 2 times less than criterion (9). The calculated i-ITB width Δ_{ITB} = ~0.2a is very close to the experimental one. The n-ITB (in the density channel) is clearly seen in Fig. 11, although there is a moderate difference between experimental and calculated density profiles.

5. Simulation of the DIIID shot #89943

Figure 13 shows the calculated and experimental profiles of temperatures T_i and T_e for t = 1.7 sec. The calculated profiles of ρ_s/L_{Ti} for t = 1.6 and 1.7 sec and experimental one for t =1.7 sec are shown in Fig. 14. At the outermost edge of the i-ITB, $\rho_s/L_{Ti} \sim 0.011$ that is close to criterion (9).

6. Simulation of the MAST shot #8575

In Figures 15-16 the calculated and experimental profiles of ion and electron temperatures at the time instants t = 0.15 and 0.2 sec are shown. The profile of the total absorbed power from two NB injectors was taken from MAST Database, which contains also the calculation results by the TRANSP code. To the instant t = 0.2 sec, the total value of the absorbed power equals to P_{NB}^{abs}=1.5 MW. The redistribution of the absorbed power between ions P_{NBi} and electrons P_{NBe} was calculated by the usual asymptotic expressions [9]. Figure 17 shows the profiles of the effective heat diffusivities, χ_i and χ_e, for ions and electrons. The ion transport barrier i-ITB is clearly seen. Its relative width $\Delta_{ITB} = \Delta\rho/a \sim 0.35$ reaches one-third of the plasma radius.

The calculated profiles of ρ_s/L_{Ti} for three time instants t = 0.1, 0.15 and 0.2 sec and the experimental one for t=0.2 sec are shown in Fig. 18. The criterion (9) is drawn also in this Figure. It is seen that there is a systematic excess of the transport barrier borders over the JET criterion (9): ρ^*_{ITB}(MAST) ≈ (1.5-1.8) ρ^*_{ITB}(JET) = 0.021-0.024.

7. Comparison of results obtained for different devices

The optimal values of the model parameters and values of other parameters characterizing the ITBs for four different devices are gathered in Table I. It is seen that the parameters C_{0i} and C_{1i}, which define the i-ITB are approximately the same for all considered devices. Also the values of χ_i inside ITB are the same for large devices with conventional aspect ratio $A \sim 3$.

TABLE I

Device and shot	C_{0i}	C_{1i}	C_{0e}	C_{1e}	χ_i inside ITB (m^2/s)	Δ_{ITB}/a model/expt	ρ^*_{ITB}
JET #40847	1	2	5	2	0.24	0.2/0.33	0.010
TFTR #94607	1.5	2	4		0.2	0.2	0.006
DIIID #89943	1	2	4		0.22	0.45	0.015
MAST #8575	1	2	>3	2	0.6	0.34	0.022

8. Conclusions

In this Report to describe the internal ITB we propose the modified Canonical profiles transport model. The model includes several parameters, which have been found by the comparison with experiment. The simulation of the shots from four devices is carried out. The model describes well the ion and electron temperature profiles including the ion-ITB. The comparison of the calculation results with JET ITB-criterion has shown that the value of ρ^*_{ITB} for different shots can differ in moderate range, $0.006 < \rho^*_{ITB} < 0.022$. The model includes the main feature of the ITBs: the negative shear diminishes the threshold power needed for the ITB formation. As a result, the proposed model is a predictive one for conventional tokamaks. It needs the additional experimental data to validate the model and make it more reliable for spherical tokamaks.

References

[1] DNESTROVSKIJ Yu.N., et al., "Canonical Profiles in Tokamak Plasmas with an Arbitrary Cross Section", Plasma Phys. Repts. **28** (2002) 887.

[2] DNESTROVSKIJ Yu.N., et al., "Development of a Transport Model for Canonical Profiles and Its Applications", Plasma Phys. Repts., **23** (1997) 566.

[3] TRESSET G., et al. "A dimensionless criterion for characterizing internal transport barriers in JET", Nucl. Fusion, **28** (2002) 520.

[4] DNESTROVSKIJ Yu.N., et al., "Application of the Canonical Profile Theory to the Problems of Heat Transport in Tokamaks", Plasma Phys. Repts. **30** (2004) 1.

[5] DNESTROVSKIJ Yu.N., et al., "Test of canonical profiles and semi-empirical transport models with JT-60U plasmas", Nucl. Fusion, **39** (1999) 2089.

[6] DNESTROVSKIJ Yu.N., et al., "Description of Transport Barriers Using the Canonical Profile Model" Plasma Phys. Repts. **24** (1998) 867.

[7] ITER Database: http://tokamak-profiledb.ukaea.org.uk/

[8] FIELD A.R., et al., "Transport in the presence of ITBs in the MAST Spherical Tokamak", Plasma Physics (Proc. 31st EPS Conf. London), CD-ROM file P4.187 and http://fusion.org.uk/eps2004/ .

[9] DNESTROVSKIJ Yu.N., KOSTOMAROV D.P., Numerical Simulation of Plasma, Springer, Berlin, 1986.

Figures

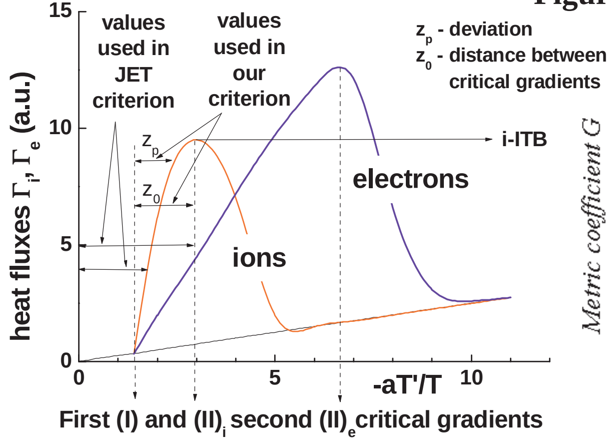

FIG. 1. The links of heat fluxes with temperature gradients and with values of z_p and z_0.

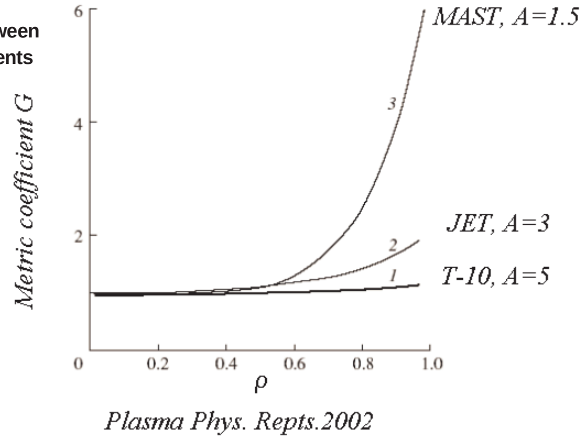

FIG. 2. Metric coefficient G in various devices.

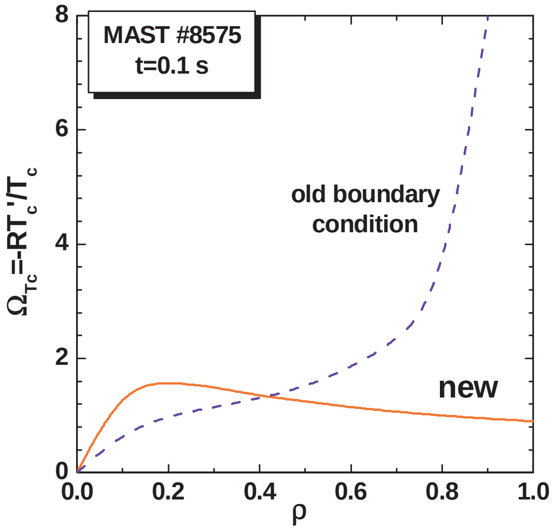

FIG. 3. Profiles of the critical gradient in MAST for old and new boundary conditions (2) and (10).

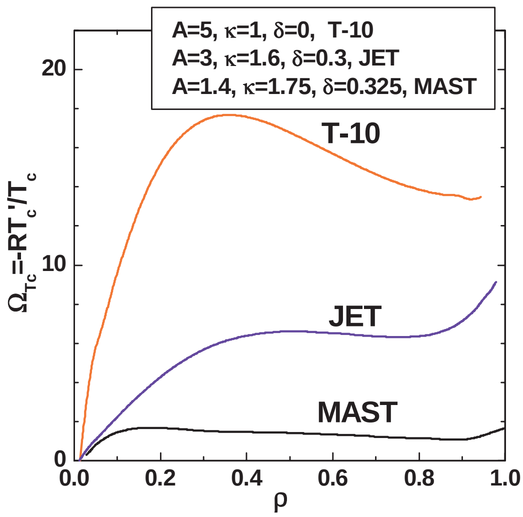

FIG. 4. Relative critical gradients of electron temperature in various devices.

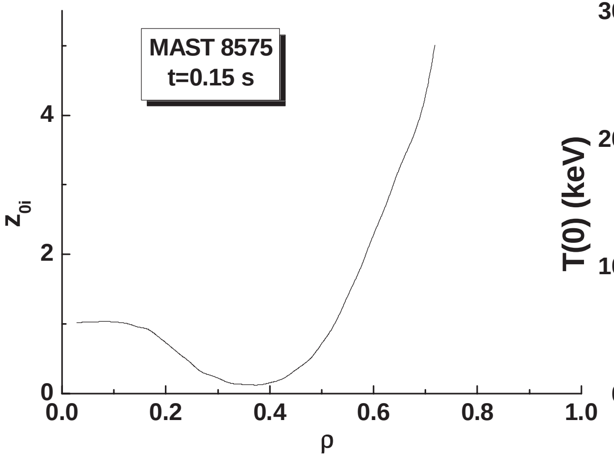

FIG. 5. Radial profile of second critical gradient in scenario with negative shear

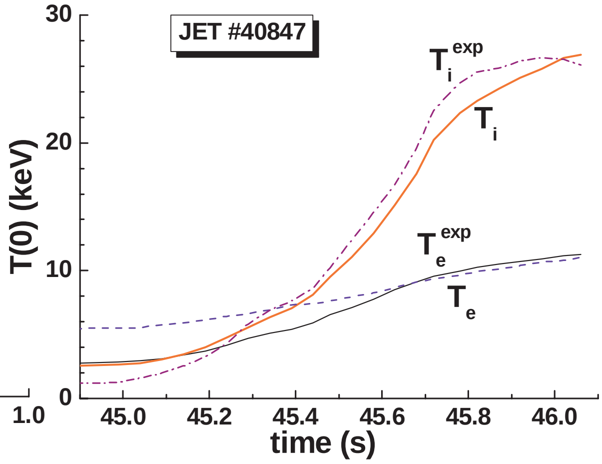

FIG. 6. Time evolution of calculated and experimental values of the central ion and electron temperatures in JET.

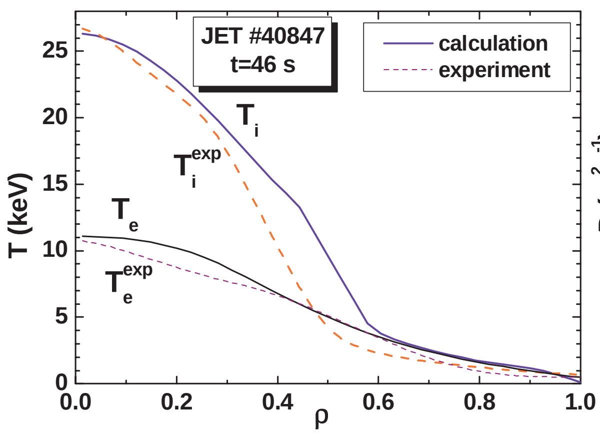

FIG. 7. The profiles of electron and ion temperatures in JET.

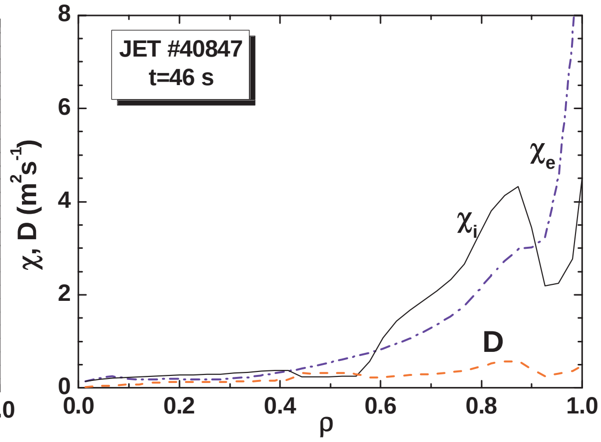

FIG. 8. The profiles of ion and electron heat diffusivities and particle diffusion in JET.

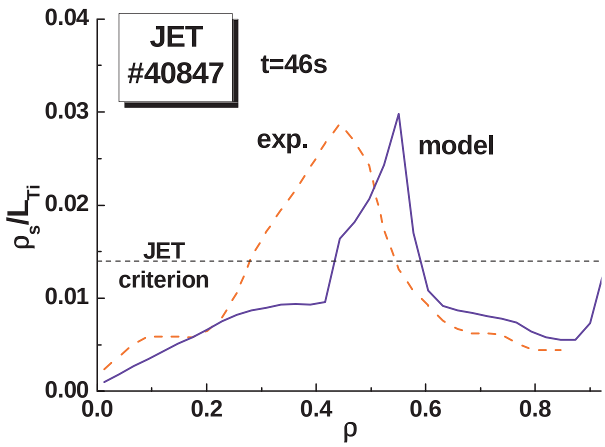

FIG. 9. The experimental and model ratios of ion sound velocity to characteristic length of ion temperatureρ_s/L_{Ti} in JET. Horizontal line shows the criterion (9)

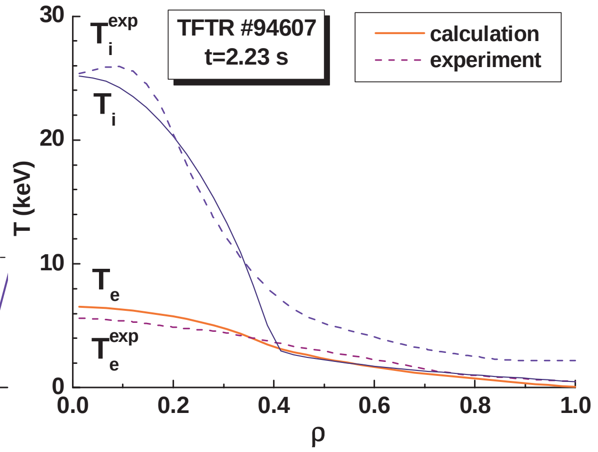

FIG.10. The profiles of ion and electron temperatures in TFTR.

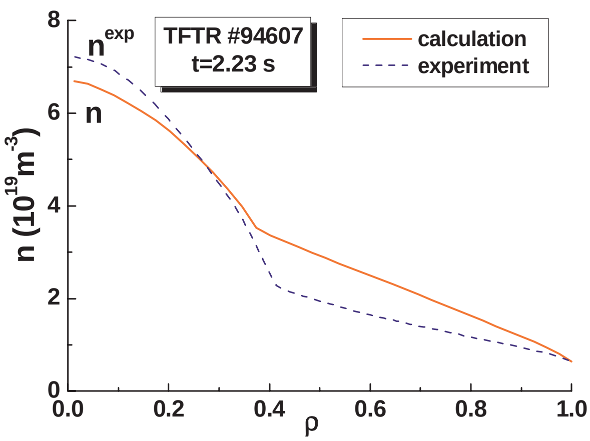

FIG. 11. The profiles of electron density in TFTR.

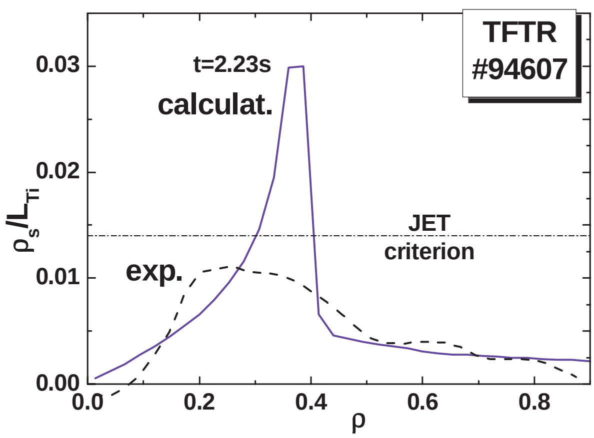

FIG. 12. The experimental and model ratios of ion sound velocity to characteristic length of ion temperatureρ_s/L_{Ti} in TFTR. Horizontal line shows the criterion (9).

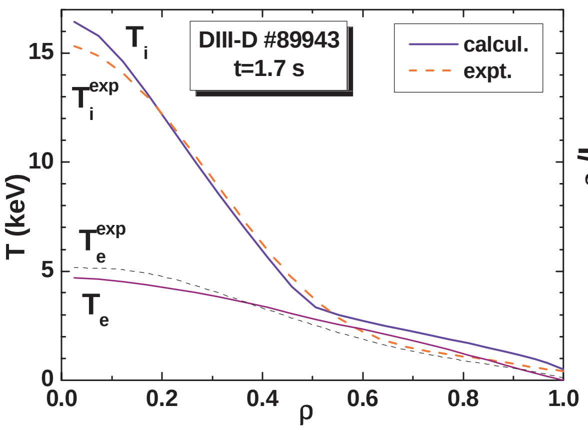

FIG. 13. The profiles of ion and electron temperatures in DIII-D.

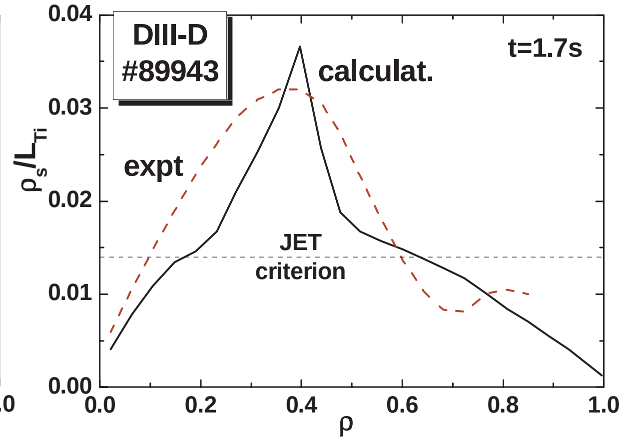

FIG. 14. The experimental and model ratios of ion sound velocity to characteristic length of ion temperature ρ_s/L_{Ti} in DIII-D. Horizontal line shows the criterion (9)

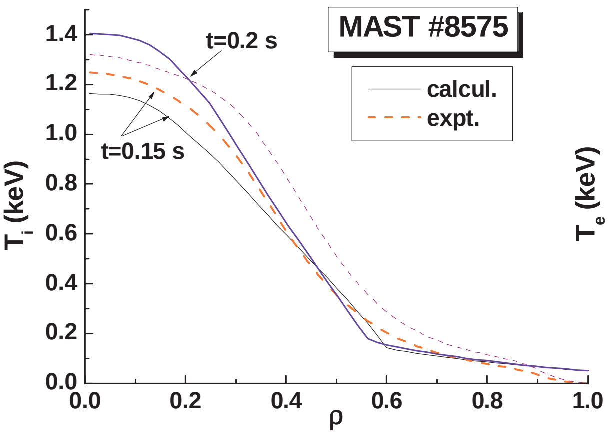

FIG. 15. The profiles of ion temperatures in MAST.

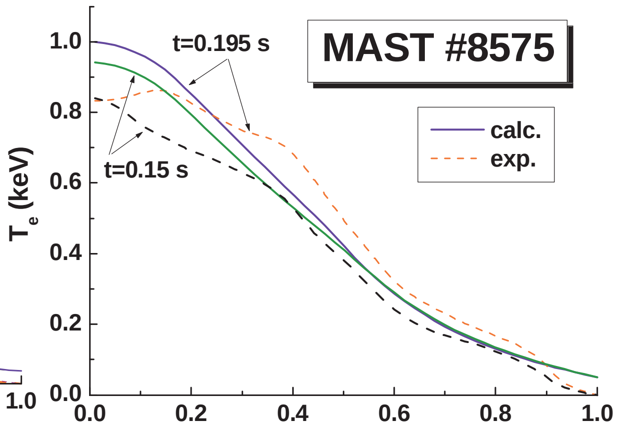

FIG. 16. The profiles of electron temperatures in MAST.

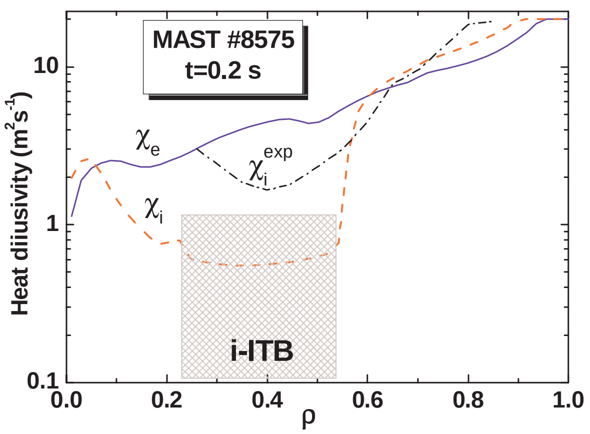

FIG. 17. The profiles of the effective heat diffusivities, χ_i and χ_e, for ions and electrons in MAST.

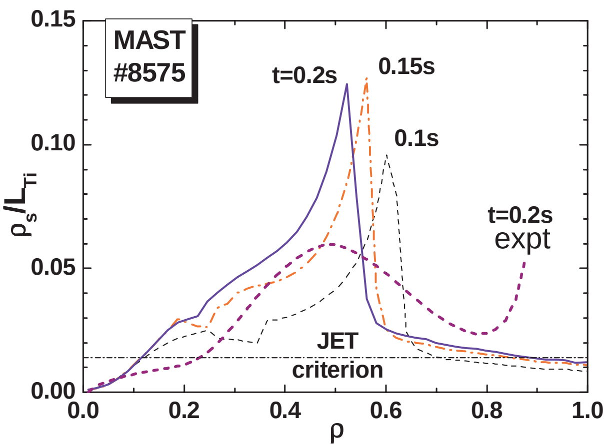

FIG. 18. The experimental and model ratios of ion sound velocity to characteristic length of ion temperature ρ_s/L_{Ti} in MAST. Horizontal line shows the criterion (9)